Optimizing the ^{8}Li yield for the IsoDAR Neutrino Experiment

Adriana Bungau, Jose Alonso, Larry Bartoszek, and Janet Conrad
Massachusetts Institute of Technology, Cambridge, Massachusetts, MA 02139, United States of America

Michael Shaevitz
Columbia University, New York, Irvington, NY 10533, United States of America

Joshua Spitz
University of Michigan, Ann Arbor, MI 48109, United States of America

(Dated: May 2, 2018)

The focus of this paper is on optimizing the electron-antineutrino source for the IsoDAR (Isotope Decay at Rest) experimental program. IsoDAR will perform sensitive short-baseline neutrino oscillation and electroweak measurements, among other Beyond Standard Model searches, in combination with KamLAND and/or other suitable detectors. IsoDAR will rely on the high-Q β^- decay of the ^{8}Li isotope for producing electron-antineutrinos, created mainly via neutron capture in an isotopically enriched ^{7}Li sleeve surrounding the Be target. In particular, this paper examines the performance, defined in terms of absolute ^{8}Li (or, equivalently, electron-antineutrino) production rate, of various candidate sleeve materials, including a lithium-fluoride, beryllium-fluoride mixture ("FLiBe") sleeve and a homogeneous mixture of lithium and beryllium ("Li-Be"). These studies show that the ^{8}Li yield can be increased substantially by employing a Li-Be sleeve and therefore motivate significant changes to the nominal IsoDAR design.

Keywords: IsoDAR; DAEδALUS; sterile neutrino; electroweak; weak mixing angle; Beyond Standard Model; non-standard neutrino interaction

I. INTRODUCTION

The three neutrino paradigm works extraordinarily well in describing mixing between the established flavor states. However, a number of fundamental questions remain. For example, a number of anomalous results, including those from LSND [1], MiniBooNE [2] and short-baseline reactor experiments [3], may be interpreted in the context of mixing involving one or more sterile neutrinos, a possibility which has excited the physics community. These inconsistencies may be explained by a (3+N) sterile neutrino model in which there are three light neutrino mass states and N massive sterile neutrino mass states.

The IsoDAR experimental program is the first stage of the DAEδALUS experiment [4, 5] and is being developed to investigate the anomalies possibly indicative of neutrino oscillations at high-Δm^2. IsoDAR represents an important technological step, in terms of producing high-power cyclotrons for a number of physics and non-physics applications, and physics reach, in the context of resolving the sterile neutrino anomaly question and providing a number of electroweak and exotic search measurements [6]. The IsoDAR experiment is based on a high intensity $\bar{\nu}_e$ source, originating from the β^- decay of ^{8}Li, coupled to a massive scintillator-based detector (e.g. KamLAND). The $\bar{\nu_e}$ can interact in the detector via the inverse beta decay (IBD) process: $\bar{\nu}_e + p \rightarrow e^+ + n$. IsoDAR will be sensitive to mapping the $\bar{\nu}_e$ ($<E> = 6.4$ MeV) disappearance oscillation wave and will study the possibility of high-Δm^2 mixing, with the unique ability to distinguish between models with one or two sterile neutrino flavors.

A. The IsoDAR experiment

The IsoDAR neutrino source is created with high current (5 mA), 60 MeV/amu H_2^+, which produces the neutrons required for the production of ^{8}Li, and resulting $\bar{\nu_e}$. An ion source is used to produce the H_2^+, which are then accelerated via a low energy beam transport system and a cyclotron, before being extracted to the target. The IsoDAR experimental program will use the high power DAEδALUS injector cyclotron to produce this intense isotope decay-at-rest antineutrino source. The neutrons produced from the H_2^+ interactions with the heavy-water-cooled ^{9}Be primary target create $\bar{\nu}_e$ from capture in an isotopically enriched (99.99%) ^{7}Li target sleeve. This degree of enrichment is needed to avoid production of tritium by neutron capture on ^{6}Li, as this cross section is several orders of magnitude larger than that of neutron capture on ^{7}Li.

Inverse beta decay interactions (IBD; $\bar{\nu}_e p \rightarrow e^+ n$) from this uniquely efficient target design are then collected by a ~ 1 kiloton scintillator-based detector at a distance of about ~ 16 m. The existing KamLAND detector would be suitable, making this proposed experiment also cost-effective compared to other approaches. Five years of running will provide nearly a million IBD events, suitable to measure the coupling parameter $\sin^2\Theta_w$ to several percent and to definitely determine if there are 0, 1, or 2 light sterile neutrinos.

II. THE CONCEPTUAL DESIGN OF THE TARGET SYSTEM

A. The current target design

The current target design [7] consists of a hollow Be cylinder leading to a circular Be disk (Fig. 1). The peak power density in the target is decreased by a wobbler magnet placed in front of the target-shielding system which spreads the beam onto its 20 cm diameter target face. The cooling system is at the back end of the target, with high pressure heavy water introduced along the central axis, and providing dissipation of the 600 kW beam power deposited on the target. The water is led away by pipes located radially around the inlet pipe.

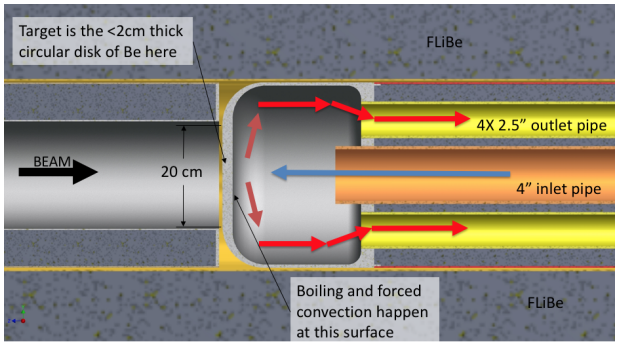

FIG. 1. Detail of the target region showing the direction of cooling water flow.

The target is surrounded by a 1 m outer diameter and 1.9 m length sleeve (Fig. 2). In the current design [7], the sleeve material is a mixture of lithium-fluoride and beryllium-floride (FLiBe), an eutectic mixture with a melting point of 459°C and a density of 1.94 g/cm^3. The low atomic weight of Li, Be, and to a lesser extent F, makes FLiBe an effective neutron moderator.

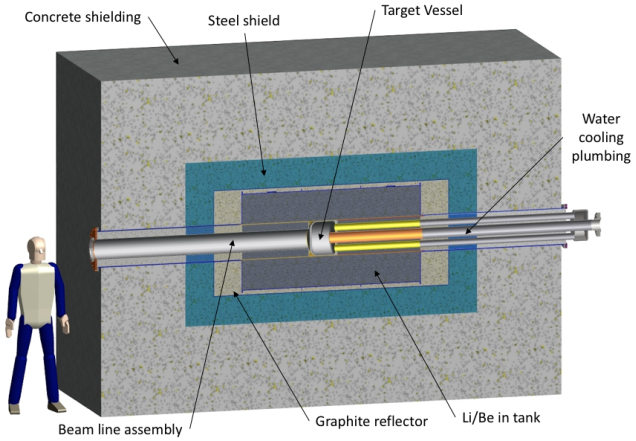

FIG. 2. Cross section of the target and shielding assembly.

FLiBe is commonly used as a coolant in molten-salt reactors. The ^{7}Li isotopic purity assumed is 99.995% although simulation studies have shown that 99.99% enrichment can meet the physics requirements of the experiment in terms of $\bar{\nu}_e$ production [8]. A 5 cm thick graphite neutron reflector surrounds the sleeve. The reflector is meant to redirect the neutrons back into the sleeve where they can be further used for ^{8}Li production. The entire target and sleeve system is enclosed in shielding, with iron inner layers and boron rich concrete outer layers.

B. The modelling of the target system

The target system is modelled using the Monte Carlo code Geant4 [9] where the hadronic interactions of incident and secondary particles with target materials, and energy ranges are defined in the physics package *particle_hp*. This package uses the *ENDF/B-VII.1* [10] and *TENDL-2014* [11] libraries for cross sections of primary and secondary particle interactions. The *ENDF/B-VII.1* library uses experimental data for projectile energies up to 150 MeV. These data are essentially nuclear reaction cross sections together with the distributions in energy and angle of secondary reaction products. The *ENDF/B-VII.1* database for proton projectiles contains data only for 48 isotopes (including Be). The *TENDL-2014* library uses some experimental data and *TALYS* [12] calculations for projectile energies up to 200 MeV. The database can be applied to all target materials but the best results are obtained for targets with atomic number in the range 12-339. The *TENDL-2014* database contains information for all isotopes.

C. ^{8}Li isotope production

The isotope production for incident 60 MeV protons on the target and sleeve configuration described is shown in Fig. 3. For a target thickness of 2 cm, the overall ^{8}Li production is 0.015 ^{8}Li per incident proton, with most of the ^{8}Li produced primarily inside the FLiBe sleeve. The Bragg peak of 60 MeV protons in Be is at 2.04 cm and the 600 kW of beam power deposited on the target can seriously affect the sustainability of the target performance in consideration of a 5 year physics run. This issue has been addressed by reducing the target thickness. The new target thickness of 1.7 cm is a compromise between maximizing neutron production and decreasing heat deposition in the Be. The ^{8}Li isotope production drops to 0.010 ^{8}Li per proton in this design, however. As the main contribution to ^{8}Li production comes from the sleeve, studies of sleeve material and geometry optimization have been performed and the results are presented below.

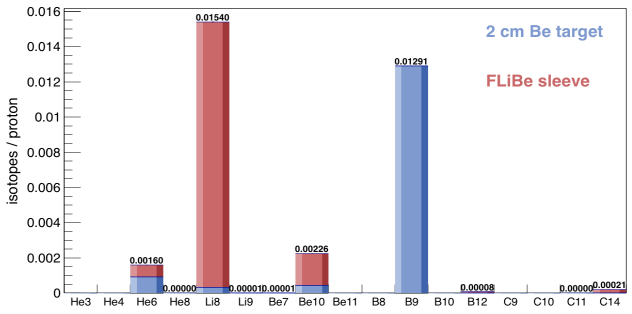

(a) 2 cm target thickness

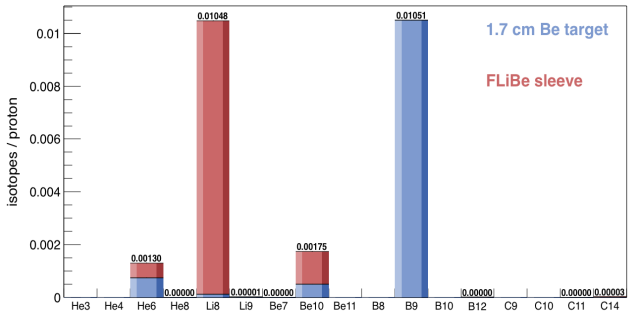

(b) 1.7 cm target thickness

FIG. 3. The ^{8}Li production in the target and sleeve, among other isotopes, for 2 cm target thickness and 1.7 cm target thickness.

III. OPTIMIZATION OF THE SLEEVE

A. Neutron interactions inside the FLiBe sleeve

The neutron interactions of interest inside the FLiBe sleeve are (1) inelastic processes in which other secondary particles are produced and (2) neutron capture processes which lead to isotope production. The ^{8}Li is produced via direct production processes like neutron capture on ^{7}Li (98.3% of the total ^{8}Li production), or by neutron inelastic interactions with Be in which a neutron and a proton are produced (1.7% of the total ^{8}Li production). The production can be increased via indirect processes in which secondary neutrons are produced with a neutron multiplication factor higher than 1. These secondary neutrons can interact at a later stage inside the sleeve and contribute to the direct ^{8}Li production processes mentioned above. The neutrons interact with all three elements present inside the sleeve; the contribution of each element to the overall ^{8}Li production is shown in Fig. 4. The energy spectra of all the neutrons interacting either inelastically or by neutron capture on Li, Be and F are shown separately in blue.

A large fraction of neutrons interact with F (80%), while a much smaller number of neutrons interact with Li (≈15%) and Be (≈5%). A fraction of these neutron interactions result in direct ^{8}Li production, and the energy spectra of these neutrons which produce ^{8}Li are shown in green in Fig. 4. The main production mechanism for these comes from the capture of <0.1 MeV neutrons on ^{7}Li (left plot). For interactions on Be, the ^{8}Li is produced in inelastic processes and the neutrons have energies above 10 MeV. Importantly, there are no processes in which ^{8}Li is produced as a result of neutron interactions with F.

Another fraction of neutrons produced inside the sleeve come from neutrons interacting inelastically and producing other secondary neutrons. The spectra of the neutrons producing additional secondary neutrons are shown separately in red. The only neutron interactions which have an average neutron multiplication factor greater than 1 are the inelastic interactions on Be. In the case of Be, for each neutron used inside the sleeve by any process - either capture or inelastic, there will be <1.35> secondary neutrons produced.

Regarding the neutron interactions on Li, there are 0.02 neutron interactions (capture or inelastic) per incident proton on target. Out of these interactions, ≈53% are low-energy neutron capture processes on ^{7}Li, and ≈47% are inelastic processes that produce additional neutrons. Regarding the neutron interactions on Be, there are 0.006 neutron interactions on Be per incident proton. Figure 4 shows that there is a significant number of low energy neutrons that are captured on Be which produce other products that are not relevant for IsoDAR. However, Be contributes to neutron multiplication as there are <1.35> neutrons produced for every neutron interaction as mentioned above. Only a small fraction of high energy neutrons produce ^{8}Li in Be. F does not contribute at all to the direct ^{8}Li production. The neutron production in F is <0.93> neutrons per neutron interaction. Therefore, the number of neutrons inside the sleeve is slightly decreased following each interaction. The first blue peak corresponds to neutron capture on F, and the second peak corresponds to inelastic neutron interactions.

Apart from the energy spectrum of the neutrons used inside the sleeve, a second factor of interest in this study is the energy spectrum of the neutrons produced in inelastic processes. These neutrons can be further used in neutron capture processes on ^{7}Li that produce ^{8}Li. Figure 5 shows the energy spectra of the neutrons that are produced in the sleeve. They are similar to the energy spectra of the neutrons which interacted inelastically to produce them, however they show a small tail towards the low energy end.

B. Neutron interactions inside the Li-Be sleeve

As the atomic ratio of Li:Be:F is 2:1:4, the presence of F drastically reduces the atomic number density of both Li and Be inside the sleeve, and therefore the number of neutron interactions with Li and Be that can produce ^{8}Li.

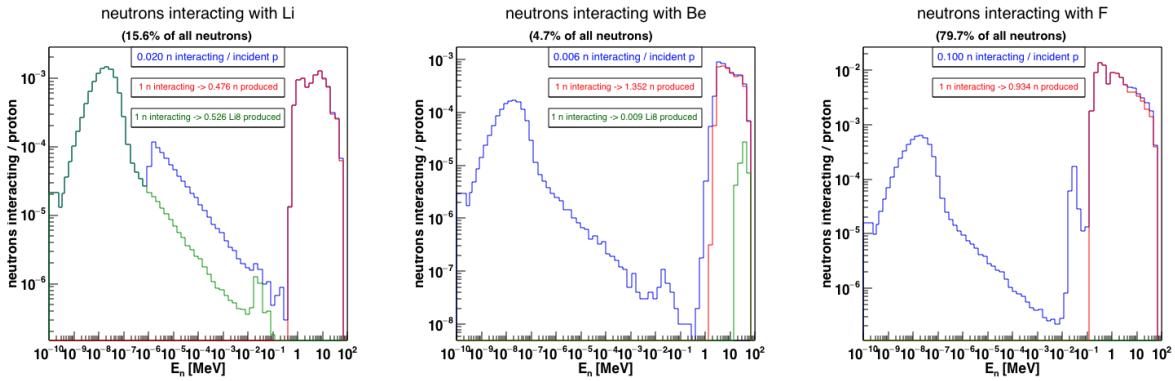

FIG. 4. The energy spectrum of all neutrons interacting inside the FLiBe sleeve is shown separately for neutron interactions on Li, Be, and F (blue). Some of the neutrons interact to produce other neutrons (red) and some interact to produce ^{8}Li (green).

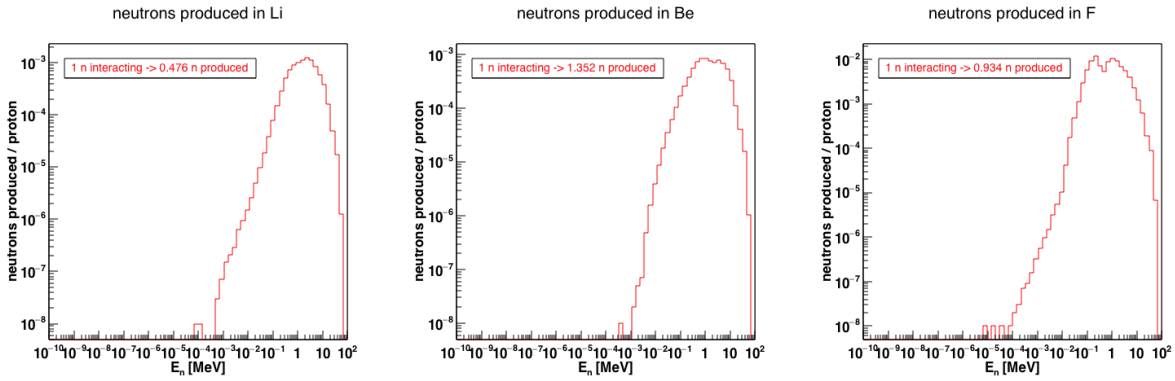

FIG. 5. The energy spectra of neutrons produced in interactions on Li, Be and F.

Since F does not contribute to direct ^{8}Li production, and the production of secondary neutrons is decreased after each neutron-F interaction, the study of material optimization has been focused on a sleeve made only of Li and Be. In order to determine the optimum composition of such a Li-Be sleeve, a parametric study for variable Be mass fraction (by weight) was performed. The results are shown in Fig. 6. As can be seen, the optimum design consists of a homogeneous mixture of enriched ^{7}Li and Be, with a Be mass fraction of 75 % (0.019 ^{8}Li per incident proton).

The ^{8}Li rates mentioned above are obtained for a homogeneous mixture of lithium and beryllium. However, in practice, a mixture close enough to homogeneity can be obtained by using small beryllium spheres immersed in lithium, and preliminary studies have shown that the ^{8}Li production increases with decreasing radius. A parametrization study of ^{8}Li yield versus radius was performed in order to find out how much the radius should be decreased and what is the correspondent value of ^{8}Li production.

Due to the complexity of the code required to simulate a very large number of Be spheres stacked inside the Li sleeve cylinder, avoiding at the same time all the inner volumes (e.g. Be vessel and cooling pipes), instead of the actual sleeve, a fixed size box of lithium of (120x120x120) cm^3 was simulated to approximate the sleeve. The box was filled with beryllium spheres of various radii. The neutrons were generated in the centre of the box using the same energy spectrum as the neutrons entering the actual sleeve.

The aim of this study was to find out how small the Be spheres have to be in order to approximate the Li-Be homogeneity, in order to ensure that the predicted ^{8}Li yields from Fig. 6 can be achieved in practice when using stacked Be spheres, rather than a homogeneous Li-Be mixture.

The results can be seen in fig. 7 and they show a continuous steadily increase in the ^{8}Li yield with decreasing sphere radius, all the way down to 1 mm radius. Below 1 mm, a plateau is reached and no further increase in the ^{8}Li yield can be observed. A homogeneous mixture of Li and Be inside the same (120x120x120) cm^3 cube was also simulated, and it was found that the ^{8}Li yield was the same as for the 1 mm radius spheres design.

The Beryllium fraction mass was calculated for each sphere radius and it was found to be $\approx$79% in all cases due to the level of compactness of the spheres regardless of their radii, value which is within the optimum range found for the homogeneous Li-Be mixture.

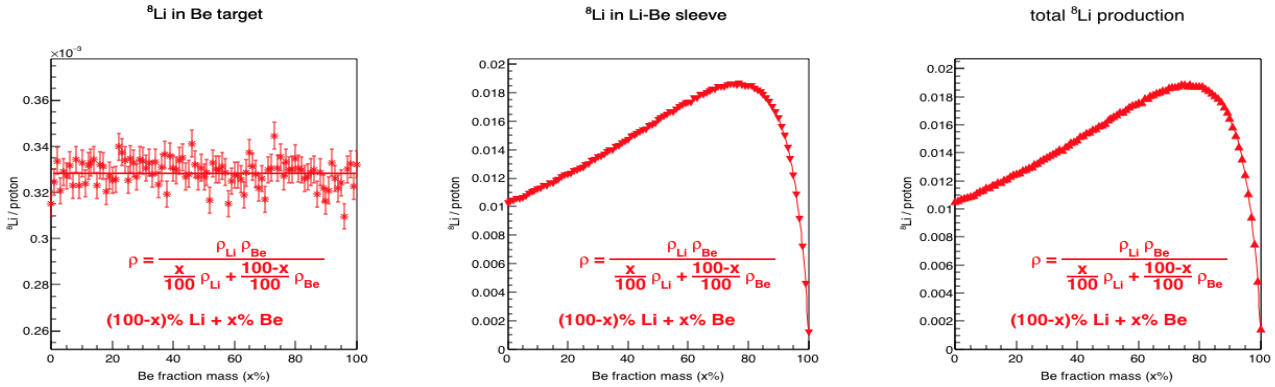

FIG. 6. The overall ^{8}Li production in the target and sleeve, for various concentrations of Li and Be.

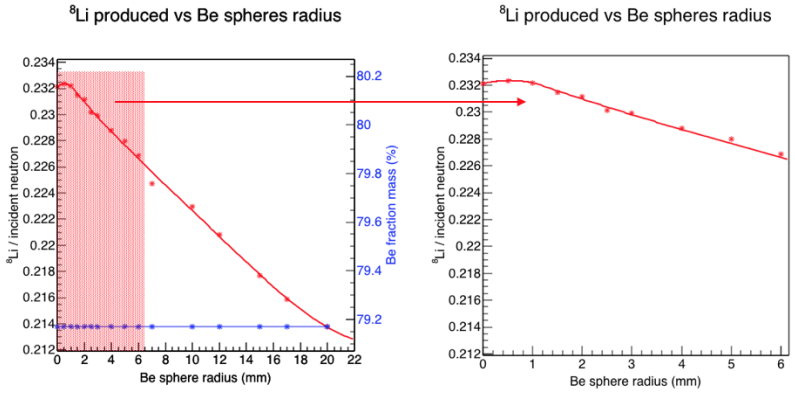

FIG. 7. The ^{8}Li production in the Li-Be cube, for various radii of the Be spheres.

If the radius is decreased from 20 mm to 1 mm, this results in a 10% increase in the ^{8}Li production. Therefore having a Li sleeve filled with Be spheres of ∼1 mm radius will result in an optimum configuration regarding the total ^{8}Li production.

In the Li-Be sleeve, the neutrons interact in the same way with Li and Be as they do with the Li and Be inside the FLiBe sleeve. However, what changes significantly is the number of neutrons interacting with Be per incident proton, and this number has increased by a factor of six (Fig. 8a). For the Li-Be sleeve there are 0.035 neutron interactions with Be per incident proton, and the average neutron multiplication factor in Be is 1.3 neutrons produced per neutron interaction. Similarly, the energy spectra of the neutrons that are produced in the sleeve is shown in Fig. 8b with a small tail towards the low energy end.

C. Change in the ^{8}Li production for two sleeve designs

Since the number of neutron interactions with the Be nuclei increases by a factor of 6 due to the increase in the atomic number density of Be inside the sleeve, the production rate of ^{8}Li from neutron inelastic interactions with Be also increases by the same factor. This can be seen in Fig. 9b. However, the number of neutron interactions with Li nuclei does not change significantly between the two target sleeves as seen in Fig. 9a. While in the case of Be interactions, the ^{8}Li is produced in inelastic processes at high neutron energies, in the case of neutron interactions on Li, the neutron capture process on ^{7}Li produces ^{8}Li, and the cross-section increases with decreasing neutron energy.

There are two distinct differences in the ^{8}Li production between the two sleeves. When F is present in the sleeve there is a high peak for neutron energies in the range 10 - 100 keV. This difference is explained in Fig. 10 which shows the energy spectrum of the neutrons lost in inelastic interactions with F (blue), and the energy spectrum of neutrons produced in these interactions (red). It can be seen that, as a result of the inelastic interactions with F, there is a surplus of neutrons in the sleeve in the energy range 1 - 100 keV. Some of these neutrons are captured on ^{7}Li, producing ^{8}Li, as there is a finite cross-section (shown in green in Fig. 10) for this process at these neutron energies.

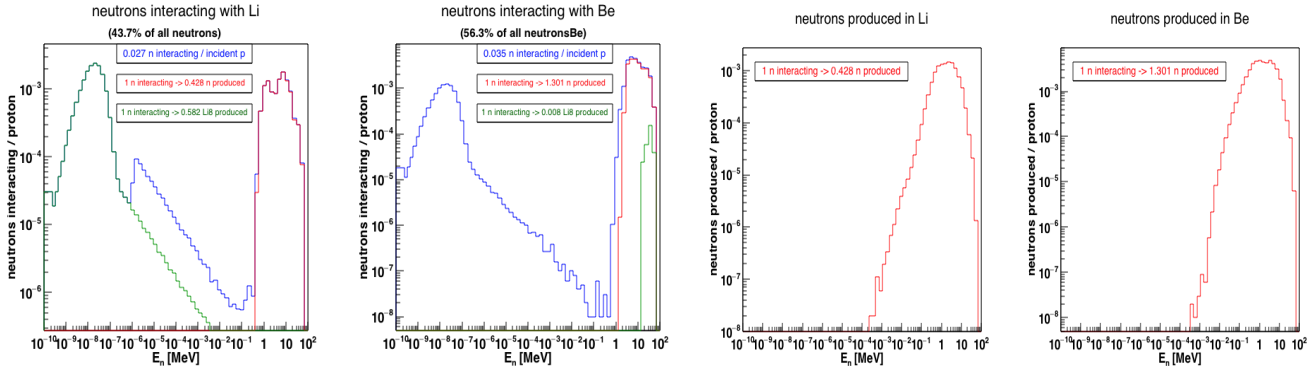

(a) neutrons interacting with Li and Be

(b) neutrons produced in Li-Be

FIG. 8. The energy spectrum of all neutrons interacting in a Li-Be sleeve with a Be mass fraction of 75%, is shown separately for neutron interactions on Li and Be (blue). A fraction of the neutrons interact producing other neutrons that can be further used (red) and a fraction interact to produce ^{8}Li (green). The energy spectra of neutrons produced in interactions on Li and Be are also shown.

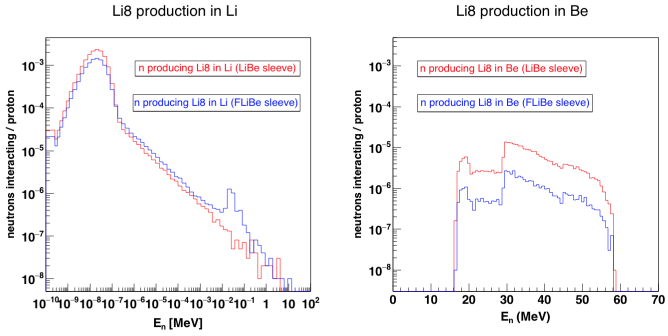

(a) ^{8}Li production in Li

(b) ^{8}Li production in Be

FIG. 9. Change in the ^{8}Li production for the two sleeve materials. The ^{8}Li production is shown separately for interactions on Li and Be.

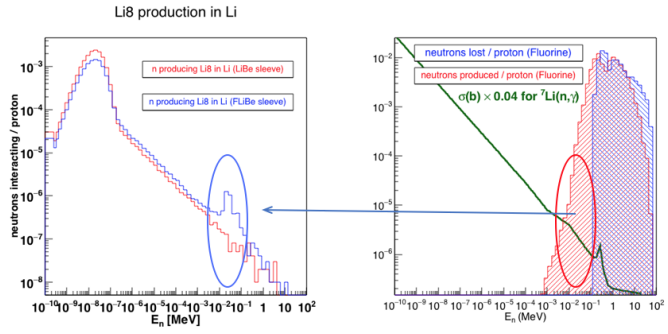

FIG. 10. An analysis of the peak in ^{8}Li production in the FLiBe sleeve.

Apart from this surplus of neutrons in the 1 - 100 keV energy range, there is also a slight decrease in the number of neutrons in the very low energy range (below 10^{-7} MeV) due to the presence of F in the sleeve (Fig. 9a). For these energies, some of the neutrons will be lost in neutron capture processes on F, so the number of interactions with ^{7}Li will also decrease when F is present.

D. Changes to the sleeve design

With the optimum sleeve composition established in terms of maximizing the ^{8}Li yield, the high cost of producing the enriched ^{7}Li sleeve requires a second optimization study of the actual size and shape of the sleeve. Therefore, we simulated a large sleeve in order to determine the regions inside the sleeve where the ^{8}Li yield is below certain threshold values. We then remove these regions while recording how this affects the total ^{8}Li production. The sleeve radius was increased to 2 m, keeping the length at 1.9 m, and the material consists of 75% mass fraction Be and 25% mass fraction Li with^{7}Li purity of 99.99%. The density as well as the Be and Li mass fractions are maintained at constant values throughout this study. Figure 11 shows a section plane cut through the sleeve, showing the shape of the sleeve while the ^{8}Li production yield threshold was varied. As the volume and mass of the sleeve were reduced, so was the overall ^{8}Li production rate. This provides an evaluation of the overall cost of the sleeve versus total ^{8}Li yield. Keeping the axes ranges fixed, one can see the continuous drop in the sleeve volume. The numerical values of the main parameters are also shown in Table I for reference.

These results show that a sleeve mass of 996 kg, corresponding to a length of 130 cm and a radius of 60 cm, results in a ^{8}Li yield above 0.016 ^{8}Li per incident proton. These results also show the optimum shape and size required for the sleeve.

Due to the technical difficulties in manufacturing a sleeve

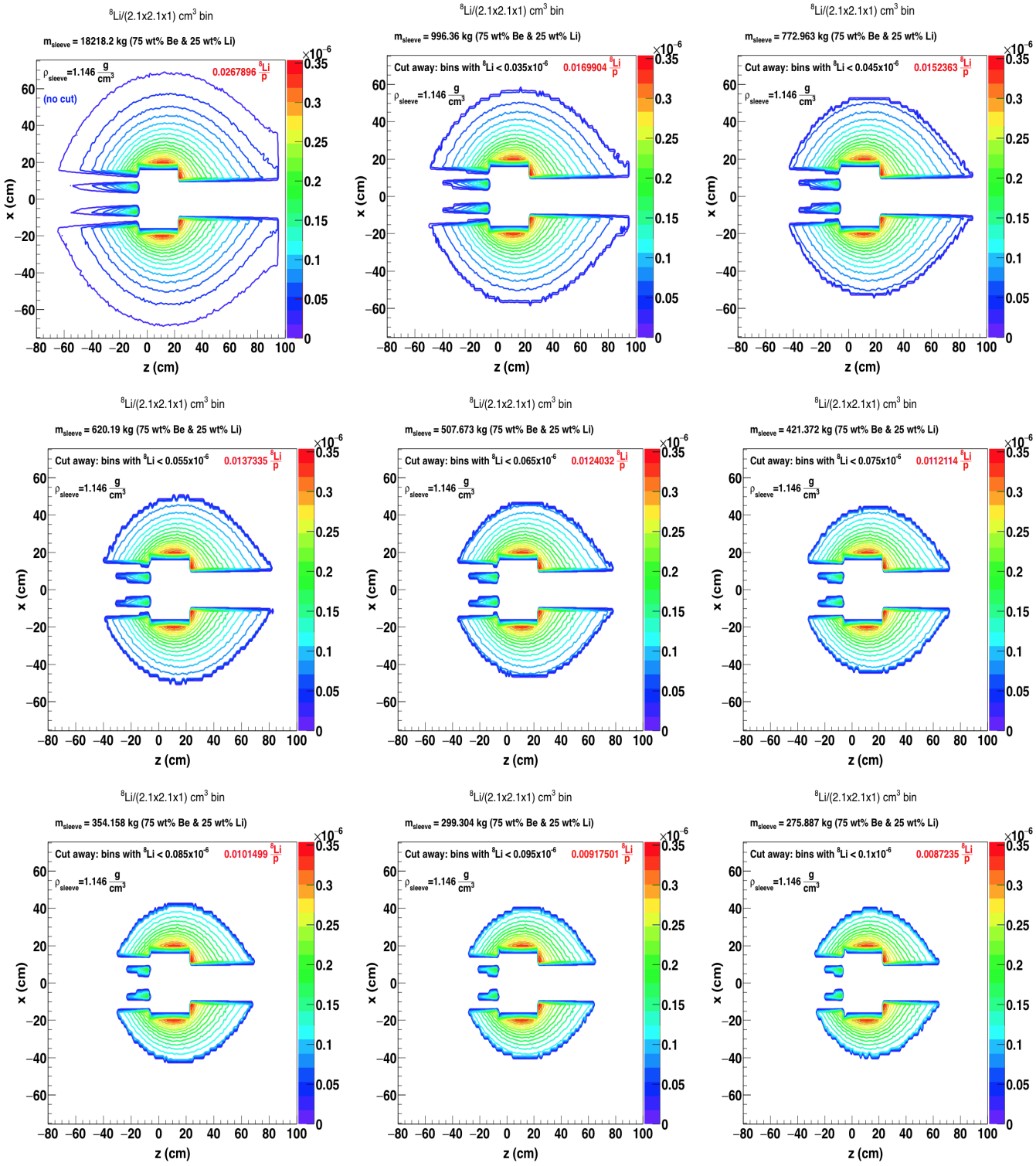

FIG. 11. Optimization of the size and shape of the sleeve. The sleeve is made of a homogeneous mixture of Li and Be (Be mass fraction is 75%). The parameters of interest are the mass of the sleeve and the corresponding ^{8}Li yield.

TABLE I. Correlation between the bin cut threshold and the total mass of the sleeve, Li mass (kg), Yield ^{8}Li/p for 99.99% ^{7}Li purity, and scale to 99.995% respectively.

Bin cut threshold	total mass (kg)	Li mass (kg)	^{8}Li yield (%)	Scale to 99.995%
0	18218.00	4554.50	2.679	3.531
3.00E-08	1148.00	287.00	1.796	2.367
3.50E-08	996.40	249.10	1.699	2.240
4.00E-08	874.00	218.50	1.608	2.120
4.50E-08	773.00	193.25	1.523	2.008
5.00E-08	689.50	172.38	1.445	1.905
5.50E-08	620.00	155.00	1.373	1.810
6.00E-08	560.00	140.00	1.305	1.720
6.50E-08	507.70	126.93	1.240	1.635
7.00E-08	461.70	115.43	1.179	1.554
7.50E-08	421.40	105.35	1.112	1.466
8.00E-08	385.50	96.38	1.066	1.405
8.50E-08	354.16	88.54	1.015	1.338
9.00E-08	325.20	81.30	0.965	1.272
9.50E-08	299.30	74.83	0.918	1.209
1.00E-07	275.90	68.98	0.872	1.149

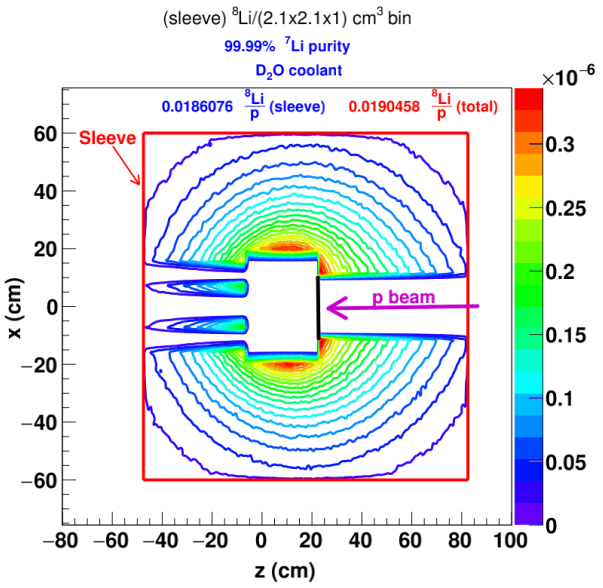

FIG. 12. The ^{8}Li production with the new cylindrical sleeve.

with a teardrop shape as shown in Fig. 11, a new, optimized cylindrical shape using the dimensions determined above has been adopted. Also, the optimal sleeve position with respect to the Be target has been determined. The results for this cylindrical sleeve are shown in Fig. 12; the ^{8}Li yield is now 0.0186 ^{8}Li per incident proton, well above the initial ^{8}Li yield which was obtained for the previous FLiBe sleeve design. The total ^{8}Li production in both the Be target and the sleeve is now 0.019 ^{8}Li per incident proton. These results are for a 2 cm thick target. When the thickness is changed to 1.7 cm, the total ^{8}Li production becomes 0.016 ^{8}Li per incident proton, which meets the physics requirements for the IsoDAR experiment.

IV. ACKNOWLEDGEMENTS

This work is supported by the National Science Foundation through grants 1505858, 1707969 and 1707971.

V. CONCLUSION

A very high flux of $\bar{\nu}_e$ will be produced by the decay of ^{8}Li for the IsoDAR experiment. The focus of this paper has been on optimizing the target-sleeve design in terms of ^{8}Li isotope production. As ^{8}Li is produced overwhelmingly inside the sleeve, two materials are considered for the sleeve that surrounds the Be target - an eutectic mixture of lithium-fluoride and beryllium-floride (FLiBe) and a homogeneous mixture of Li-Be. A detailed study of neutron interactions on each chemical element inside the two sleeve materials shows that Li-Be performs better. The study shows that F in FLiBe, apart from drastically reducing the atomic number density of both Li and Be inside the sleeve, and therefore the number of neutron interactions with Li and Be, does not contribute to ^{8}Li production and the number of secondary neutrons produced after each neutron-F interaction is slightly decreased. The Be mass fraction for which the ^{8}Li yield is maximized is 75%. This can be achieved in practice by having a Li sleeve stacked with Be spheres with a radius of up to 1 mm. With this sleeve material and Li-Be mass fractions as above, a size and shape sleeve optimization study was performed. By removing areas with ^{8}Li yield below a certain threshold, a teardrop sleeve shape was obtained. For a sleeve mass of of 996 kg, the ^{8}Li yield is above 0.016 ^{8}Li per incident proton. With the new sleeve design, the total ^{8}Li yield is 0.019 ^{8}Li per proton for a 2 cm thick target and 0.016 ^{8}Li per proton for a 1.7 cm thick target.

[1] Aguilar A*et al.* LSND Collaboration, "Evidence for Neutrino Oscillations from the Observation of $\bar{\nu}_e$ Appearance in a $\bar{\nu}_\mu$ Beam", Phys. Rev. D 64, 112007 (2001).
[2] A.A. Aguilar-Arevalo *et al.* [MiniBooNE Collaboration], "Improved Search for $\bar{\nu}_\mu \to \bar{\nu}_e$ Oscillations in the MiniBooNE Experiment", Phys. Rev. Lett. 110, 161801 (2013).
[3] G. Mention, M. Fechner, Th. Lasserre, Th. A. Mueller, D. Lhuillier, M. Cribier, and A. Letourneau, "Reactor Antineutrino Anomaly", Phys. Rev. D 83, 073006 (2011).

[4] Bungau,A./ *et al.* "Proposal for an Electron Antineutrino Disappearance Search Using High-Rate ^{8}Li Production and Decay", Phys. Rev.Lett. 109, 141802 (2012).

[5] J.M. Conrad and M.H. Shaevitz, "Multiple Cyclotron Method to Search for CP Violation in the Neutrino Sector", Phys. Rev. Lett. 104, 141802 (2010).

[6] J.M. Conrad, M.H. Shaevitz, I. Shimizu, J. Spitz, M. Toups, and L. Winslow, "Precision $\bar{\nu}_e$-electron Scattering Measurements with IsoDAR to Search for New Physics "

[7] IsoDAR Collaboration, "IsoDAR at KamLAND: A Conceptual Design Report for the Technical Facility", Draft for the KamLAND Collaboration, Sept. (2015).

[8] A. Bungau, R. Barlow, M.H. Shaevitz, J. Alonso, J.M. Conrad, and J. Spitz, "Optimization Studies of a High Intensity Electron Antineutrino Source", Proceedings of IPAC2013, Shanghai, China (2013).

[9] S. Agostinelli *et al.*, "Geant4: A Simulation Toolkit" Nucl. Instr. Meth. A 506, 250 (2003).

[10] M. B. Chadwick, M. Herman, P. Oblozinsky, *et al.*, "ENDF/B-VII.1 nuclear data for science and technology: Cross sections, covariances, fission product yields and decay data", Nuclear Data Sheets, 112(12):2887-2996 (2011).

[11] "TENDL-2014: TALYS-based evaluated nuclear data library", A.J. Koning, *et al.*, www.talys.eu/tendl-2014.html

[12] A. Koning, D. Rochman, "Modern Nuclear Data Evaluation With The TALYS Code System", Nuclear Data Sheets 113, 2841 (2012).